Secondary Control Strategies for Frequency Restoration in Islanded Microgrids with Consideration of Communication Delays

Ahumada, Constanza; Cardenas, Roberto; Saez, Doris; Guerrero, Josep M.

Published in:
I E E E Transactions on Smart Grid

DOI (link to publication from Publisher):
10.1109/TSG.2015.2461190

Publication date:
2016

Secondary Control Strategies for Frequency Restoration in Islanded Microgrids with Consideration of Communication Delays

Constanza Ahumada, Roberto Cárdenas, *Senior Member, IEEE,* Doris Saez, *Senior Member, IEEE,* and Josep M. Guerrero, *Fellow, IEEE*

***Abstract*— One of the well-known methods to share active and reactive power in microgrids, is droop control. A disadvantage of this method is that in steady state the frequency of the microgrid deviates from the nominal value, and has to be restored using a Secondary Control System (SCS). The signal obtained at the output of the SCS is transmitted using a communication channel to the generation sources in the microgrid, correcting the frequency. However, communication channels are prone to time delays which should be considered in the design of the SCS; otherwise, the operation of the microgrid could be compromised. In this paper, two new SCSs control schemes are discussed to deal with this issue: a Model Predictive Controller (MPC) and a Smith predictor based controller. The performance of both control methodologies are compared to that obtained using a conventional PI-based SCS using simulation work. Stability analysis based on small signal models and participation factors is also realised. It is concluded that in terms of robustness, the MPC has better performance.**

Index Terms* — *Droop Control, Microgrid Control, Model Predictive Control, Smith Predictors.

I. Introduction

One of the advantages of MicroGrids (MGs) is the capability of operating isolated from a main grid. To achieve this, necessarily the demanded power has to be shared between all the units in the MG [1]–[3]. The usual method to accomplish active and reactive power sharing is to use *Q-V* and *P-f* droop control algorithms [2], [4]–[7].

When *Q-V* and *P-f* droop control systems are used [8], active and reactive power sharing is achieved but in steady state the system frequency and voltage are not necessarily the nominal values [2]–[4], [9], [10]. Therefore a Secondary Control System (SCS) [2], [11] is usually required to correct the frequency and voltage. Additionally, secondary control algorithms can be used for reactive power compensation [12] and to reduce the harmonic content of the voltage waveform [13]. In other studies, it is proposed to eliminate secondary control to restore the frequency, for instance using a smart transformer [14] (which is a rather bulky solution) or using a modified droop control which changes mainly the phase of the Distributed Generation Resources (DGRs), without affecting much the MG frequency [15]. However, the stability issues related to this control method have not been addressed at all in any publication. Moreover, phase control is possible only when static power converters are used, because with conventional generators the inertia does not allow the implementation of this control methodology. Additional information about these control methodologies is discussed in the review papers [6], [7].

In general terms SCSs can be distributed [16]–[18] or centralised [19], [20], with both topologies being depicted in Fig. 1. In the centralised control strategy the frequency is usually estimated by a PLL and compared with the reference value. A controller is used to process this error, producing a correcting signal ω_s which is transmitted to all the DG units in the system (see Fig. 1a). A typical distributed control DSC is shown in Fig. 1b, in this case each generating unit is provided with secondary control capacity in order to correct the voltage and frequency deviations of each DGR. Moreover, each DGR in Fig. 1b is equipped with PLLs and transducers to measure or estimated the frequency, voltage and power at the DGR Point of Common Coupling (PCC).

Distributed secondary control systems have been recently proposed in the literature [21]–[24]. However in most of these papers some sort of centralised control system is still required.

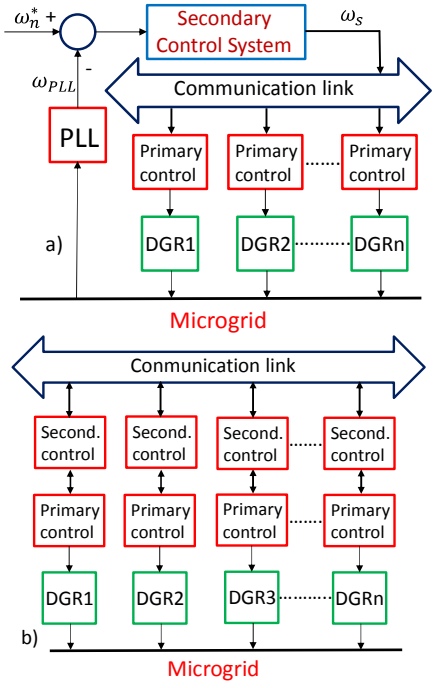

Fig. 1. Secondary control system topologies for frequency regulation. a) Centralised SCS. b) Distributed secondary control system.

C. Ahumada, R. Cárdenas and D. Sáez are with the Faculty of Mathematical and Physical Sciences, University of Chile, Av. Tupper 2007, 8370451, Santiago Chile (e-mail: rcd@ieee.org, dsaez@ing.uchile.cl).

J. Guerrero is with the Institute of Energy Technology, Aalborg University, 9220 Aalborg, Denmark (e-mail: joz@et.aau.dk).

This work has been partially supported by FONDECYT 1140775, Advanced Center for Electrical and Electronic Engineering, Basal Project FB0008, and Fondequip EQM130058.

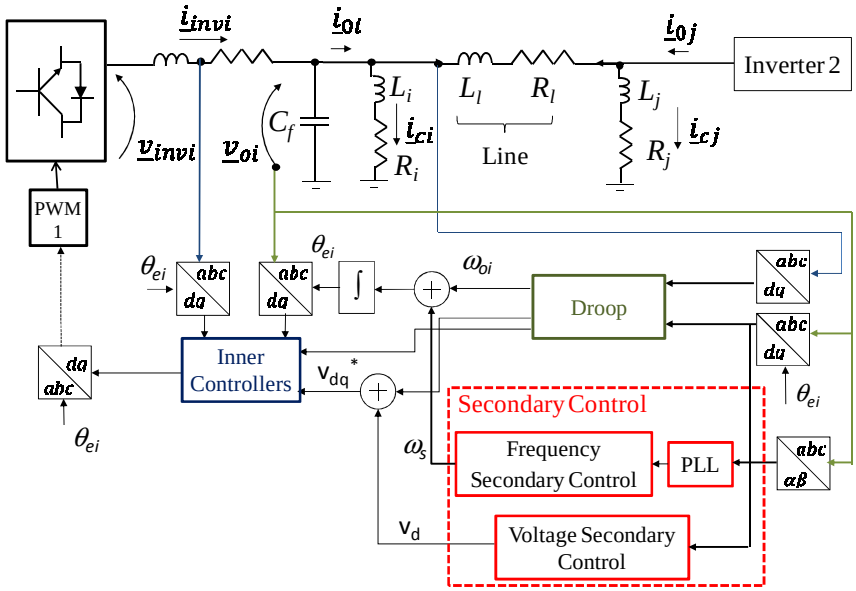

Fig. 2. Microgrid topology discussed in this work.

For instance in [22] a master/slave control system is proposed to improve the sharing of active power.

In this paper the use of a CAN network is required for the master-DGR to transmit power references and synchronising signals to all the slave generating units (i.e. a kind of centralised control is implemented by the master-DGR). To the best of our knowledge, the only work where a highly distributed SCS is presented is [21]. However, some sort of centralised control is still required in this method for black start of the microgrid.

Even when the performance of the proposed distributed SCSs looks promising, the issues and problems inherent to this topology have not been fully investigated yet. Some of the issues which need to be addressed are:

- Centralised SCSs can operate using a unidirectional low bandwidth communication channel. On the other hand, in the distributed SCS proposed in [21], each of the SCS requires information about the voltages and frequencies measured by the other DGR units at the PCC. Therefore, for a relatively large microgrid, the use of a high bandwidth bidirectional communication link is mandatory. Moreover, as discussed in [22], in some applications time synchronisation signals have to be provided between the units (e.g. to coordinate the sampling of the variables). The use of these signals and the high bandwidth required by distributed SCSs could compromise the MG robustness.
- As discussed in [9], the electrical frequency is a global signal in a microgrid. Therefore if several controllers are regulating the grid frequency the stability of the system could be compromised. To the best of our knowledge the stability of highly distributed SCSs has not been analysed yet.

One of the reported advantages of distributed SCS is robustness in the presence of communication delays. This has been reported in [21], considering an experimental system of two DGRs. However, with only two generating units is difficult to obtain a general conclusion, considering that each DGR has to obtain information of only one additional DGR in the system. If the MG has a large number of generating units, all of them exchanging information through the communication channel, it is likely that the impact of the communication delays is going to be much more important.

In summary as discussed in [21] , the future application of highly distributed SCSs is auspicious and they could be a good option in systems where high bandwidth bidirectional communication channels are available at a relatively low cost. However, at the present centralised controllers could be still considered more robust and reliable than distributed SCSs, particularly in microgrids located in developing countries and/or rural areas where good communication infrastructure is not always available [25]. As stated in [7] communication is crucial for centralised controllers and it failure could lead to a system collapse. Therefore, in this paper centralised DSCs, which can achieve robust performance in the presence of variable and unknown communication delays, are discussed. The communication delay is assumed between the controller and the DGRs.

One of the controllers proposed in this work is based on a Model Predictive Control (MPC) algorithm. Additionally a secondary control system based on a Smith Predictor (SP) is also analysed in this work. The performance of these control algorithms is studied considering their dynamic response and robustness. The former is analysed considering a MATLAB/SIMULINK model of the microgrid (see Fig. 2), with the primary control systems being implemented using synchronous rotating *d-q* coordinates. Stability issues are analysed considering the system eigenvectors. The participation factor method [26] is used to determine the influence of the state variables on a particular eigenvector (or vice versa).

The control systems of the MG depicted in Fig. 2, are shown at the bottom of that graphic. Droop control, load voltage control and current control have to be provided to both inverters. Because of simplicity, only the control systems associated with the left side VSI are shown in Fig. 2. The voltage and current controllers are embedded in the block labelled “inner” control.

At the bottom right of Fig. 2, the SCS is shown. A Phase Locked Loop (PLL) is used to estimate the MG frequency. This value is compared with the nominal frequency and the error is processed by a controller. This is further discussed in Section IV. Fig. 2 also shows the secondary voltage control loop which is considered outside the scope of this paper. Further information about voltage restoration control is presented elsewhere [6], [7].

The rest of this work is organised as follows. In Section II a brief review of droop control is realised. In Section III the control strategies for the primary control system are briefly discussed. In Section IV the proposed secondary control strategies are introduced and analysed. In Section V a closed loop analysis for stability studies is derived. In Section VI simulation results are presented. Finally, in Section VII an appraisal of the control methods discussed in this work is presented at the conclusions.

II. Droop Control System

In MGs, the sharing of active power is typically achieved by changing the phase angle between the DGR voltage outputs. This is further explained using the well-known expression:

$$P_{ij} = 3\frac{v_i v_j}{x_{ij}}\sin(\delta_{ij}) \qquad (1)$$

Where P_{ij} is the active power transferred from the power source "i" to the power source "j", (v_i, v_j) are the voltage moduli of both power sources, δ_{ij} is the phase angle shift between the two voltage vectors and x_{ij} is the equivalent reactance between the two nodes in the microgrid.

The phase angle δ_{ij} is modified as a function of the active power supplied for each load. This is usually accomplished using droop control where the frequency is regulated using:

$$\omega_{0i} = \omega_{cf} - m_{pi}P_{if} \qquad (2)$$

Where, m_{pi} is the droop slope, ω_{cf} is a function of the maximum frequency deviation allowed in the system (see [11]), ω_{0i} is the output frequency of the i^{th} power source, and P_{if} is the mean power supplied to the MG by the same power source.

In this work, it is assumed that the impedance between power sources (x_{ij}) [see (1)] is inductive. If the impedance is not inductive some of the methods, e.g the ones proposed in [2], [3], [9], [27]–[31], have to be used. The analysis and discussion of these control methods are considered outside the scope of this work and the interested reader is referred elsewhere [2], [3], [9], [27]–[31].

Using (2), the phase angle δ_{ij} between generating units is modified according to:

$$\delta_{ij} = \int(\omega_i - \omega_j)\,dt \qquad (3)$$

Therefore if a load step is applied anywhere, e.g. at the output of the power source "j", the control system of this unit will change its output frequency. Finally, in steady state, the system will settle down to a new operating point where the MG frequency is not necessarily equal to the nominal value ω_n. The SCS regulates the frequency of the MG eliminating the deviation from the nominal frequency ω_n which is introduced by the *P-f* droop control algorithm [2], [3], [9].

As mentioned before, centralized SCS requires a communication channel to send a correcting signal ω_s to the inverters. In this case the output frequency of each inverter is:

$$\omega_i = \omega_{0i} + \omega_s \qquad (4)$$

The secondary control system is usually designed with a low control bandwidth in order to ensure decoupling from the primary control loops implemented in each power source. Otherwise, the stability of the whole system could be jeopardised.

III. Primary Control System for the Microgrid

In this paper secondary control of the microgrid voltage and the tertiary control level are considered outside the scope of this work. The interested reader is referred elsewhere [2], [6], [7], [25], [32], [33].

A. Voltage and Current Control Systems.

The current and voltage control of each VSI is shown in Fig. 3. Each inverter has a voltage control loop implemented in *d-q* coordinates and orientated along the load voltage vector. The outputs of the voltage controllers are the current references i_d^* and i_q^* which are processed by the internal current control loops [34]. As it is standard practice, the current control loops are about 10 times faster than the voltage control loops [35]. The electrical angle θ_{ei} is obtained by integrating the electrical frequency of (4). In Fig. 3 decoupling terms are included to allow decoupled design of the *d* and *q* axis voltage and current controllers. Notice that standard PI controllers are used in the inner control loops, since in steady state the *d-q* voltages/currents are dc signals.

B. Primary Control.

As mentioned before, in this work it is assumed that the impedance between the inverters is inductive; therefore, power sharing is achieved by modifying the phase angle between the inverter voltage vectors (see (1)) using droop control. However, before using (2), the output power P_i of each inverter is filtered-out using a low pass filter. This allows a relatively good decoupling between the droop

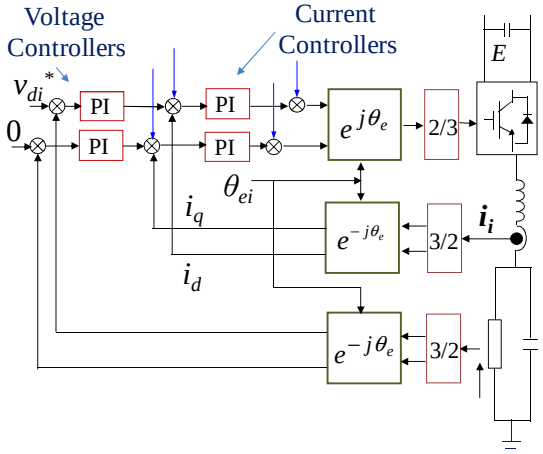

Fig. 3. Voltage and currents control systems.

control and the voltage/current control systems, improving the overall stability of the system.

Using the voltage and current vectors, the power can be calculated in the stationary α-β frame or synchronous rotating d-q coordinates using:

$$P_i = k\,(\underline{v}_{invi} \odot \underline{i}_{invi}) \tag{5}$$

where k is dependent on the abc to α-β transformation being used and the symbol $\odot$ stands for the inner product between the voltage and current vectors. Filtering out the power calculated from (5) is achieved using:

$$P_{if} = \frac{\omega_c}{s+\omega_c}\,P_i \tag{6}$$

The value of P_{if} calculated from (6) is used in (2). Using the output of the SCS (ω_s), the angle θ_{ei} is calculated as:

$$\theta_{ei} = \int(\omega_{0i} + \omega_s)dt \tag{7}$$

The angle θ_{ei} is used in the vector control system of Fig. 3 to transform from α-β to d-q and vice versa.

IV. Secondary Control System for Regulating the Microgrid Frequency

Fig. 4 shows a typical SCS implemented using a PI controller. It is assumed in this case that the communication channel has a delay of τ_d seconds. It is important to highlight that, unlike the delays usually used in power electronic system (which are in the order of µs), communication delays can easily achieve values in the order of milliseconds or even tens of milliseconds [36], [37]. The SCS usually requires a PLL to estimate the MG operating frequency ω_i and a controller to process the error between the nominal frequency ω_n and ω_i. This is shown in Fig. 4 where the SCS is enclosed in a dashed box.

Notice that in Fig. 4, the dynamics of the fast primary control system are neglected. Therefore, assuming that the control systems are decoupled, the characteristic equation of the SCS is obtained as:

$$1 + e^{-s\tau_d}G_pG_cH = 0 \tag{8}$$

Where $e^{-s\tau_d}$ is the transfer function of the communication delay; G_c is the PI controller; H is the PLL transfer function; and G_p is the system plant. Using (8) and some linear design control techniques as Bode or Evan's Root Locus, the controller can be designed. However, the decoupling between the SCS and the primary control system can only be assumed when the SCS is well designed and tuned. i.e. (8) is only valid when ω_{0i} (see Fig. 4) could be considered as an external disturbance to the SCS. Moreover, if the communication delay is uncertain and changes in a relatively large operating range, a conventional controller (usually a PI) could not be robust enough to ensure good and stable operation of the SCS in all the operating conditions.

As mentioned before, in this paper two robust control strategies are studied as alternatives to the PI controller: a PI controller enhanced with a Smith predictor (SP), and a model predictive control (MPC) strategy. The secondary control system depicted in Fig. 4, which is based on a PI controller, is considered as the base case for this study.

A. Controller Based on Smith Predictor (SP)

A block diagram of a PI controller enhanced with a Smith Predictor is shown in Fig. 5. The complete control system is enclosed in the dashed box at the bottom of that graphic.

To implement the Smith predictor, good estimations of the transfer functions of the plant ($\hat{G}_p(s)$) and delay ($\hat{G}_d(s)$), in a typical operating point are required.

Using Fig. 5, the closed loop transfer function between $\omega_i(s)$ and $\omega_n(s)$ is:

$$\frac{\omega_i(s)}{\omega_n(s)} = \frac{\frac{PI(s)G_p(s)G_d(s)}{1+PI(s)\hat{G}_p(s)\hat{H}(s)}}{1+\frac{PI(s)F(s)}{1+PI(s)\hat{G}_p(s)\hat{H}(s)}\left(\hat{G}_p(s)\hat{H}(s)\hat{G}_d(s)-G_p(s)H(s)G_d(s)\right)} \tag{9}$$

Assuming $\hat{G}_p(s)\hat{H}(s)\hat{G}_d(s) \approx G_p(s)H(s)G_d(s)$, the transfer function of (9) is simplified to:

$$\frac{\omega_i(s)}{\omega_n(s)} = \frac{PI(s)G_p(s)G_d(s)}{1+PI(s)\hat{G}_p(s)\hat{H}(s)} \tag{10}$$

Therefore when good estimates $\hat{G}_p(s)$, $\hat{G}_d(s)$ and $\hat{H}(s)$ are used, the delay $e^{-s\tau_d}$ does not affect the closed loop characteristic equation (i.e. the denominator of (10)). Using (10), it is simple to design a controller using some of the well-known methods reported in the literature. To improve the controller performance when operating with a non-exact plant model (or unknown system delay) a low pass filter could be used in the Smith predictor feedback [38] [39].

B. Model Based Predictive Controller (MPC)

The model based predictive control is based on an optimisation of the future system behaviour with respect to the

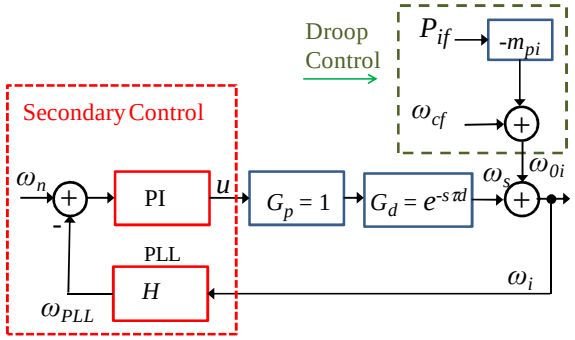

Fig. 4. Conventional Secondary Control System to regulate the frequency.

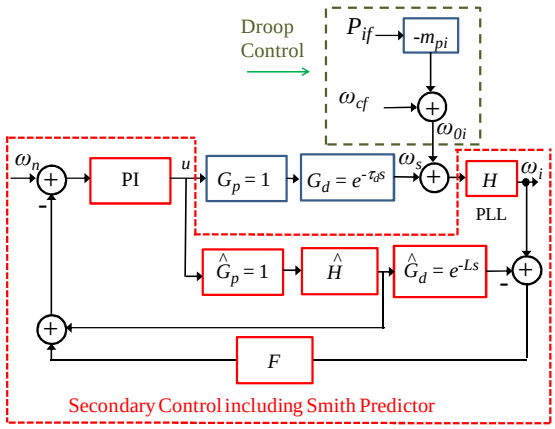

Fig. 5. Frequency secondary control with a SP controller.

future values of the control actions [40], [41]. For the MPC proposed in this work, a discrete model of the system is used to predict the future behaviour; and a set of future control actions are calculated by optimising a cost function with constraints on the manipulated and controlled variables. An explicit solution can be obtained if the cost function is quadratic, the model is assumed linear, and there are no constraints.

In this work, predictive control is proposed to implement the SCS in order to mitigate the stability issues produced by the delays, as shown in Fig. 6. In particular, good design of MPC systems allows dealing with variable and uncertain delays [41].

The cost function used in this work is given by (11);

$$J = \sum_{j=N_1}^{N_2}[\omega_{PLL}(t+j|t) - \omega_n]^2 + \lambda \sum_{j=1}^{N_U}[\Delta u(t+j-1)]^2 \quad (11)$$

it generates the control action ω_s at the SCS output. The first term minimizes the tracking error between the prediction of the measured system frequency and its set-point ω_n, and the second term minimizes the control action effort. λ is an weighting factor value, which in this work has been selected to obtain similar SCS bandwidth for MPC to that achieved for the other SCS strategies studied in this work. N_1 and N_2 are the minimum and maximum prediction horizons respectively, and N_U is the control horizon [41].

To obtain the prediction of the system frequency required for the MPC designed, as shown in Fig. 6, the following expression is used:

$$\omega_{PLL} = HG_p e^{-\tau_d s} u \quad (12)$$

where u is the control action of the MPC secondary frequency control. Equation (12) could be discretised and represented as an Auto Regressive Integrated with eXogenous variable (ARIX) model given by [41]:

$$\omega_{PLL}(t) = \frac{B(z^{-1})}{A(z^{-1})}u(t-1) + \frac{\xi(z^{-1})}{\Delta} \quad (13)$$

Where $A(z^{-1})$ and $B(z^{-1})$ are polynomials, $\Delta = 1 - z^{-1}$ and $\xi(t)$ is assumed as white noise. The term $\frac{\xi(z^{-1})}{\Delta}$ represents unknown disturbances. Therefore, minimizing (11) with the model defined in (13), the resulting MPC control action is:

$$\Delta u(t) = \frac{P(z^{-1})}{Q(z^{-1})}\omega_{PLL} \quad (14)$$

$P(z^{-1})$ and $Q(z^{-1})$ are polynomials obtained from the analytical solution of the minimization of J.

From (13)-(14) the characteristic equation of the SCS based on a MPC strategy is obtained as:

$$A(z^{-1})\Delta Q(z^{-1}) - B(z^{-1})z^{-1}P(z^{-1}) = 0 \quad (15)$$

V. Stability Analysis

As mentioned above, the performance of the proposed control systems is analysed considering the dynamic performance of the SCS and the performance in the presence of uncertainties in the communications delay. In this work, the symbol L denotes the delay, which has been assumed for SCS designing purposes; while the symbol τ_d stands for the real communication delay.

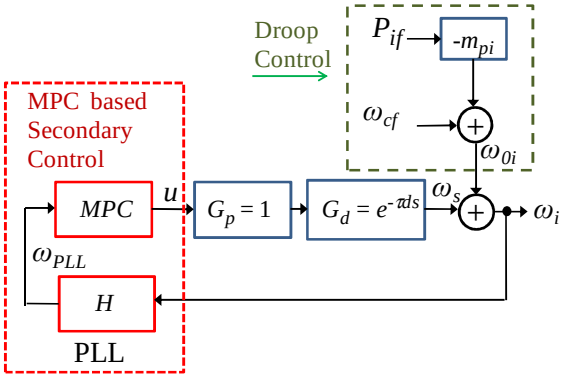

Fig. 6. Frequency secondary control with a MPC controller.

To study the stability of the system, the state equations associated to the primary and secondary control are derived in this section. For each SCS algorithm (designed with a given delay L), the maximum plant delay, τ_d, for a stable system is calculated.

The state equations for the primary control loops have already been discussed in [31], [33]. For completeness, a brief analysis is presented in the next sections.

A. Primary Control System.

The modelling is obtained from the MG topology of Fig. 2. The voltage and currents are represented as vectors in α-β or d-q coordinates, e.g:

$$\underline{i}_{oi} = i_{oi\alpha} + j i_{oi\beta} \quad (16)$$

$$\underline{i}_{oi} e^{-j\theta_{ei}} = i_{oid} + j i_{oiq} \quad (17)$$

$$\underline{i}_{oi} = (i_{oid} + j i_{oiq}) e^{j\theta_{ei}} \quad (18)$$

Where θ_{ei} is obtained using (7). In this work, the state equations of the MG are obtained using d-q coordinates. The state equation of the voltage/current control systems depicted in Fig. 3 are not included in this section, because they are considered well known. Moreover, only the equations of DGR "i" and those describing the transmission line dynamics are presented below. The state equations corresponding to inverter "j" are similar. However to transform from α-β to d-q and vice versa, the angle θ_{ej} instead of θ_{ei} has to be used.

1) Dynamic Related with Inverter "i",

The state equations describing the dynamic of the inverter output current, filter capacitor voltage and load current are [33]:

$$\Delta i_{invid} = \omega_i \Delta i_{inviq} + I_{inviq}\Delta\omega_i - \frac{R_{fi}}{L_{fi}}\Delta i_{invid} + \frac{\Delta v_{invid}}{L_{fi}} - \frac{\Delta v_{oid}}{L_{fi}} \quad (19)$$

$$\Delta i_{inviq} = -\omega_i \Delta i_{invid} - I_{invid}\Delta\omega_i - \frac{R_{fi}}{L_{fi}}\Delta i_{inviq} + \frac{\Delta v_{inviq}}{L_{fi}} - \frac{\Delta v_{oiq}}{L_{fi}} \quad (20)$$

$$\Delta \dot{i}_{cid} = \omega_i \Delta i_{ciq} + I_{ciq}\Delta\omega_i - \frac{R_i}{L_i}\Delta i_{cid} + \frac{\Delta v_{oid}}{L_i} \quad (21)$$

$$\Delta\dot{i}_{ciq} = -\omega_i \Delta i_{cid} - I_{cid}\Delta\omega_i - \frac{R_i}{L_i}\Delta i_{ciq} + \frac{\Delta v_{0iq}}{L_i} \quad (22)$$

$$\Delta\dot{v}_{0id} = \omega_i \Delta v_{0iq} + V_{0iq}\Delta\omega_i + \frac{\Delta i_{invid}}{C_{fi}} - \frac{\Delta i_{0id}}{C_{fi}} \quad (23)$$

$$\Delta\dot{v}_{0iq} = -\omega_i \Delta v_{0id} - V_{0id}\Delta\omega_i + \frac{\Delta i_{inviq}}{C_{fi}} - \frac{\Delta i_{0iq}}{C_{fi}} \quad (24)$$

2) Transmission Line Dynamics

The dynamic of the current $\underline{i}_{oi} - \underline{i}_{ci}$ are described by the following state equations:

$$\Delta\dot{i}_{0id} = \omega_i \Delta i_{0iq} + I_{0iq}\Delta\omega_i - \frac{R_l}{L_l}\Delta i_{0id} + \left(\frac{1}{L_l} + \frac{1}{L_i}\right)\Delta v_{0id} - \frac{\Delta v_{0jd}}{L_l} + \left(\frac{R_l}{L_l} - \frac{R_i}{L_i}\right)\Delta i_{cid} \quad (25)$$

$$\Delta\dot{i}_{0iq} = -\omega_i \Delta i_{0id} - I_{0id}\Delta\omega_i - \frac{R_l}{L_l}\Delta i_{0iq} + \left(\frac{1}{L_l} + \frac{1}{L_i}\right)\Delta v_{0iq} - \frac{\Delta v_{0jq}}{L_l} + \left(\frac{R_l}{L_l} - \frac{R_i}{L_i}\right)\Delta i_{ciq} \quad (26)$$

3) State Equations for Droop Control

Before obtaining these state equations, linearization of (5) is required, i.e:

$$P_i = k\left(v_{invid} i_{invid} + v_{inviq} i_{inviq}\right) \quad (27)$$

$$\Delta P_i = k(\Delta v_{invid} I_{invid} + \Delta v_{inviq} I_{inviq} + V_{invid}\Delta i_{invid} + V_{inviq}\Delta i_{inviq}) \quad (28)$$

The state equations are obtained from (2), (6) and (28) as:

$$\Delta\dot{P}_{if} = \omega_c \Delta P_i - \omega_c \Delta P_{if} \quad (29)$$

$$\Delta\dot{\theta}_{ei} = \Delta\omega_s - m_{pi}\Delta P_{if} \quad (30)$$

B. Secondary Control with SP Strategy

Using Fig. 5, it can be shown that the dynamic behaviour of the Smith Predictor based SCS is given by the following expressions:

$$\omega_i = \omega_s + \omega_{0i} = \omega_s + \omega_n - m_{pi}P_{if} \quad (31)$$

$$\omega_s = G_d G_p PIe \quad (32)$$

$$e = \omega_n - \left(\hat{H}\hat{G}_p PIe + F\left(H\omega_i - \hat{G}_p\hat{H}\hat{G}_d PIe\right)\right) \quad (33)$$

Using the equations (31)-(33), the secondary controller is described by:

$$\omega_s\left(1 + \hat{H}\hat{G}_p PI - F\hat{G}_p\hat{H}\hat{G}_d PI + G_d G_p FHPI\right) = \left(G_d G_p PI - G_d G_p FHPI\right)\omega_n + G_d G_p FHPI m_{pi} P_{if} \quad (34)$$

Considering $\hat{H} = H$, $\hat{G}_p = G_p = 1$, $G_d = e^{-\tau_d s}$ and $\hat{G}_d = e^{-Ls}$, the state space representation is derived. Then, the state space model for the secondary control can be represented by:

$$\dot{X}_{S_{SP}} = A_{F_{SP}} X_{S_{SP}} + B_{FP_{SP}} P_{if} \quad (35)$$

Matrixes $A_{F_{SP}}$ and $B_{FP_{SP}}$ are presented in Appendix *A*. Therefore, the state space model of the MG of Fig. 2, considering the SCS shown in Fig. 5, is given by:

$$X = \left[X_1^T, X_2^T, X_{S_{SP}}^T\right]^T \quad (36)$$

$$\dot{X} = A_{SP} X \quad (37)$$

With:

$X_1 = \left[\Delta\delta_1, \Delta P_1, \Delta Q_1, \Delta\phi_{1dq}, \Delta\gamma_{1dq}, \Delta I_{c1dq}, \Delta I_{inv1dq}, \Delta V_{01dq}, \Delta I_{01dq}\right]^T$

$X_2 = \left[\Delta\delta_2, \Delta P_2, \Delta Q_2, \Delta\phi_{2dq}, \Delta\gamma_{2dq}, \Delta I_{c2dq}, \Delta I_{inv2dq}, \Delta V_{02dq}, \Delta I_{02dq}\right]^T$

and

$X_{S_{SP}} = \left[\Delta\omega_s^{(4)}\ \Delta\ddot{\omega}_s\ \Delta\ddot{\omega}_s\ \Delta\dot{\omega}_s\ \Delta\omega_s\right]^T$

C. Secondary Control with MPC Strategy

For the MPC, the closed loop transfer function is obtained replacing the equation (15) in (14).

$$\frac{\left(\Delta A(z^{-1})Q(z^{-1}) - B(z^{-1})z^{-1}P(z^{-1})\right)}{Q(z^{-1})}\omega_{PLL} = \frac{\Delta A(z^{-1})B_H(z^{-1})}{A_H(z^{-1})}P_{if} \quad (38)$$

Equation (38) is transformed to the continuous domain and the state space model is derived as:

$$\dot{X}_{PLL_{MPC}} = A_{F_{MPC}} X_{PLL_{MPC}} + B_{FP_{MPC}} P_{if}$$
$$Y = C_{F_{MPC}} X_{PLL} + D_{FP_{MPC}} P_{if} \quad (39)$$

Considering MPC, the state space model of the MG and primary/secondary control systems is given by:

$$X = \left[X_1^T, X_2^T, X_{S_{MPC}}^T\right]^T \quad (40)$$

$$\dot{X} = A_{MPC} X \quad (41)$$

Where X_1 and X_2 have been defined above. The vector $X_{S_{MPC}}$ is defined as:

$X_{S_{MPC}} = \left[\Delta\omega_{PLL}^{(6)}\ \Delta\omega_{PLL}^{(5)}\ \Delta\omega_{PLL}^{(4)}\ \Delta\ddot{\omega}_{PLL}\ \Delta\ddot{\omega}_{PLL}\ \Delta\dot{\omega}_{PLL}\ \Delta\omega_{PLL}\right]^T$

D. Eigenvalue Analysis

To study the stability of the system, the state space models for the primary and secondary control with SP and MPC strategies are considered. Specifically the eigenvalues of the matrices A_{SP} and A_{MPC} are determined (see Appendix A). Then, participation factor analysis is used to associate each eigenvalue to its most relevant system state. Analytically, the participation factor F_{Pij}, which relates the eigenvalue j with the state i, is given by:

$$F_{Pij} = \phi_{ij}\psi_{ji} \quad (42)$$

With ϕ_j the right eigenvector associated to the eigenvalue j, and ψ_j the left eigenvector associated to the eigenvalue j.

The controllers to be studied in this work are tuned for a MG with the parameters presented in Appendix *B*. The resulting controller parameters are presented in the Appendix *C*. In Table I the natural frequency ω; the bandwidth BW; the damping factor ξ; and t_s the settling time are presented. These values have been obtained using participation factor analysis. The design have been realised considering a delay $L = 0.1[s]$. Notice that the secondary controllers have been designed with similar bandwidth, in order to allow a comparison on similar basis.

The robustness of each secondary control method is studied using small signal analysis. The controllers are designed for L=0.1[s] and for each SCS strategy the maximum delay τ_{dmax} which allows a stable system is calculated. These values are depicted in Table I (see τ_{dmax}). Notice that the MPC is more robust allowing a maximum communication delay of $\tau_{dmax} = 1.11[s]$.

TABLE I
CONTROLLERS CHARACTERISTICS OBTAIN WITH SMALL SIGNAL ANALYSIS

Controller	$\omega\left[\frac{rad}{s}\right]$	$BW\left[\frac{rad}{s}\right]$	ξ	$t_s[s]$	$\tau_{dmax}[s]$
Inner Voltage	42.87	-	0.99	0.10	-
Inner Current	401.21	-	1	0.01	-
PI	2.7676	3.27	1	1.63	0.83
SP	3.3024	3.25	1	1.36	0.88
MPC	1.6618	3.29	1	2.71	1.11

In Figs. 7 and 8, the system eigenvalues are shown, for the SCSs based on SP and MPC. The variation on the eigenvalue positions respect to the variation on the communication delay is plotted. The arrows indicates increasing values of τ_d. For both control methodologies, it is observed that the poles near the origin are the ones associated to the SCSs. Therefore these are the poles producing unstable behaviour, when the communication delay is increased beyond τ_{dmax}.

VI. SIMULATION EXPERIMENTS

Beside of the stability analysis, simulation work has been used to study the dynamic performance of the MG depicted in Fig. 2, considering the secondary control systems proposed in this paper. A more detailed view of the microgrid used in the simulation work is depicted in Fig. 9. The parameters used in the simulation work are shown in Table II.

Again the SCSs are designed for a given value of L, and tested for several communication delays τ_d.

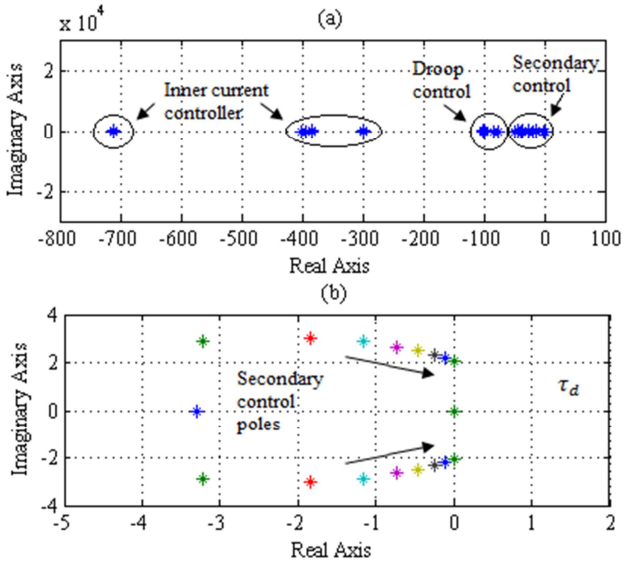

Fig. 7. (a) Poles movement due to an increase in the plant delay working with SP. (b) Zoom of the poles movement.

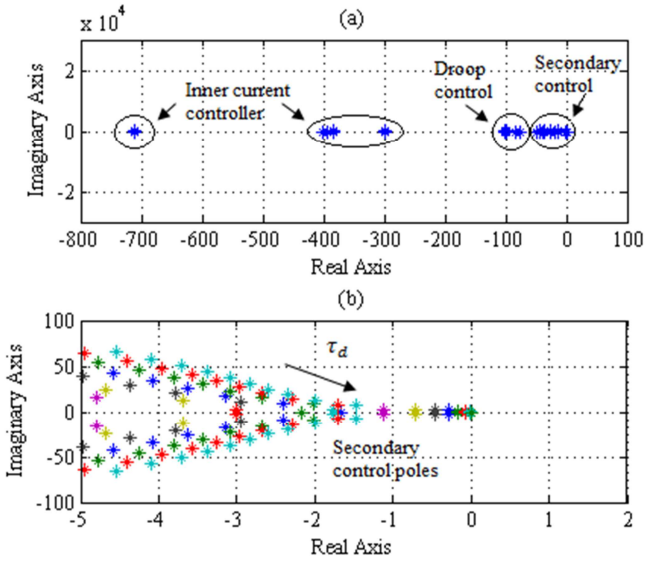

Fig. 8. (a) Poles movement due to a change in the plant delay working with MPC. (b) Zoom of the poles movement

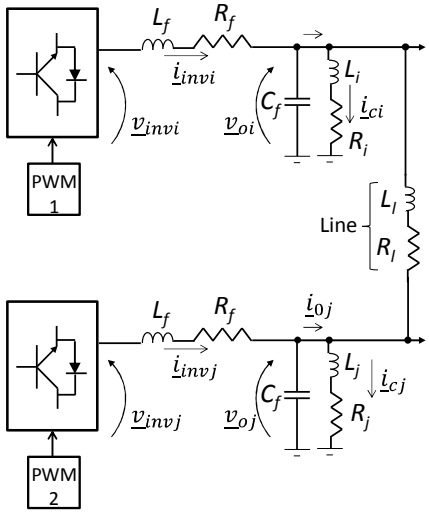

Fig. 9. Microgrid used in the simulation work presented in this section.

TABLE II
MICROGRID PARAMETERS

Parameter	Value	Unit
Line Resistance (R_l)	0.1	$[\Omega]$
Line Inductance (L_l)	7.2	$[mH]$
Filter Resistance (R_f)	0.1	$[\Omega]$
Filter Inductance (L_f)	1.8	$[mH]$
Filter Capacitance (C_f)	25	$[\mu F]$
Nominal Voltage (v_{01}-v_{02})	220	$[V_{RMS}]$
Nominal Frequency	50	$[Hz]$
PLL time constant	0.05	$[s]$
Communication delay (nominal)	0.1	$[s]$
Maximum active power inverter 1	1800	[W]
Maximum active power inverter 2	1800	[W]
Maximum reactive power inverter 1	1265	[Var]
Maximum reactive power inverter 2	1265	[Var]

A. Performance of the Primary Control System

The results presented in this sections are obtained for a designed delay $L = 0.1[s]$. The SCS are tested considering a plant delay of $\tau_d = 0.1[s]$.

Fig. 10 shows the primary control results for active power and voltage using PI, SP and MPC strategies in the SCS. Fig. 10a shows a load step connection achieving 85% of the maximum load capacity of the system and Fig. 10b corresponds to a load disconnection from 85% to 50% of the maximum capacity. More information about these power steps is presented in Table V of the Appendix B.

From Fig. 10 it is concluded that there is virtually no difference in the performance of the primary control system when different secondary control methods are used. This validated the design strategy because the control loops have been designed for decoupled operation and this is achieved by all the SCS strategies studied. Fig. 10 shows that both inverters generate the same active power even though the loads connected in parallel to each of them are different. This is due to the use of the same droop control slope in both inverters. In addition, Fig. 10 shows that the settling time of the active power is approx. 0.05[s], which is well approximated to the settling time of $t_s = 0.06[s]$ obtained from the small signal model analysis.

The tests corresponding to Fig. 10 have been repeated considering controllers designed for L=0.1[s] and $\tau_d = 0.6[s]$. Again, the performance of the primary control system is good and the time response obtained from these tests are very similar to those depicted before. Therefore, it is concluded that unless the real part of the eigenvalues are very close to the right half-plane, the performance of the primary control system is adequate and fully decoupled from the SCS performance.

B. Performance of the Secondary Frequency Control with Uncertainties in the Communication Delays

The parameters of the designed secondary frequency controllers are presented in the Appendix *C* (see Table VII) for nominal delay times of $L = 0.1[s]$ and $L = 0.2[s]$. In this section, the dynamic performance of the SCS strategies is presented and their robustness analysed.

The results obtained for the SCS implemented with PI, SP and MPC strategies are depicted in Tables III and IV. In this tables MOV is the percentage of overshoot; t_s is the settling time; and J_T is an error index given by equation (43).

$$J_T = J_f + \lambda J_U \tag{43}$$

$$J_f = \frac{1}{T_{sim}} \sum_{k=1}^{N} (\omega(k) - \omega_n)^2 \tag{44}$$

$$J_U = \frac{1}{T_{sim}} \sum_{k=1}^{N} \left(\omega_s(k) - \omega_s(k-1)\right)^2 \tag{45}$$

Where λ is the parameter used in the predictive control; and J_f and J_U are terms associated to the regulation and control of the system, ω, ω_s, and ω_n are the system frequency, the SCS output, and the nominal frequency respectively; T_{sim} is the simulation time; and N is the time period.

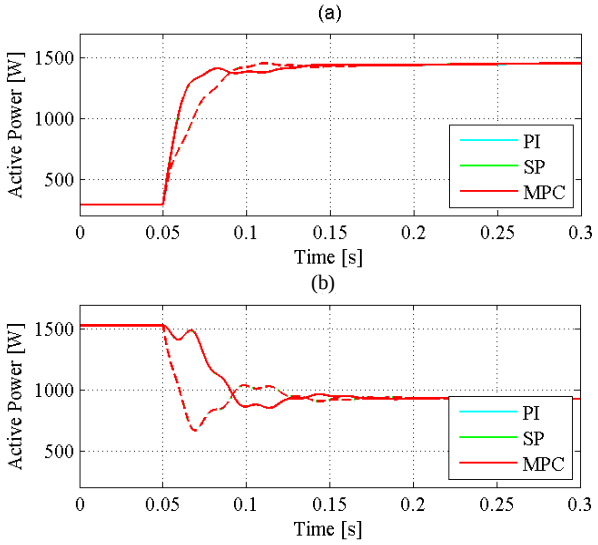

Fig. 10. Active power in inverter 1 (continue line) and inverter 2 (dashed line) for a) Load connection. b) Load disconnection ($\tau_d = 0.1[s]$).

From Table III, is concluded that for a designed delay $L = 0.1[s]$ and an increasing plant delay τ_d, the overshooting, the settling time, and J_T increase for all the controllers. For the case of the MPC, the change in J_T is smaller, allowing the system to maintain stable eigenvalues for a wider τ_d range.

TABLE III
SECONDARY FREQUENCY CONTROL WITH $L = 0.1[s]$

Controller	$\tau_d[s]$	J_T	$MOV[\%]$	t_s [s]
PI		4.284	0.000	1.029
SP	0.100	2.775	0.000	1.224
MPC		3.093	0.000	1.861
PI		7.805	0.100	2.426
SP	0.400	5.266	0.060	1.900
MPC		4.641	0.000	1.328
PI		11.894	0.160	6.490
SP	0.500	7.069	0.120	4.260
MPC		5.391	0.040	2.340
PI		24.636	0.220	>20.000
SP	0.600	10.410	0.160	7.560
MPC		6.379	0.060	2.700
SP	0.700	16.239	0.220	>15.000
MPC		7.746	0.100	4.420
MPC	0.900	9.494	0.120	16.500
MPC	1.100	22.762	0.200	>19.000

Moreover, from the results shown in Table III it is concluded that the PI strategy cannot be used (because of stability issues) for a delay $\tau_d = 0.7[s]$, while the SP cannot be used when the delay is $\tau_d = 0.9[s]$. These values are comparable to those obtained using small signal stability analysis, which are discussed in Section V.D (see τ_{dmax} in Table I.).

It was expected to obtain the lower J_T with the MPC based SCS, because this controller is usually designed to minimize this index, nevertheless, SP has lower values of J_T for a nominal τ_d. This is due to the fact that the predictive control system presented in this work has been designed to obtain the same bandwidth of the other SCS strategies; i.e. it has not been designed to minimize J_T as it is typical for this controller family. Nevertheless, as the delay τ_d increases, the J_T obtained

with MPC becomes considerably lower than that obtained using the other control strategies.

Table IV presents the results for the designed delay $L = 0.2[s]$ tested with different plant delays. From this table it is concluded that the settling time increases as the plant delay decreases. Notice that (when the delay is lower than that used for designing purposes) the PI control strategy achieves the lowest settling times for all the cases followed by the SP and the MPC.

TABLE IV
SECONDARY FREQUENCY CONTROL WITH $L = 0.2[s]$

Controller	$\tau_d[s]$	J_T	$MOV[\%]$	$t_s\,[s]$
PI		5.001	0.000	0.892
SP	0.200	3.378	0.000	0.982
MPC		3.761	0.000	1.972
PI		4.284	0.000	1.025
SP	0.100	2.775	0.000	1.223
MPC		3.358	0.000	2.141
PI		3.622	0.000	1.19
SP	0.010	2.423	0.000	1.41
MPC		3.131	0.000	2.35

Fig. 11 presents the frequency for both inverters under a load connection (see Figs. 11a, 11b, and 11e) and load disconnection (see Figs. 11c and 11d) for a plant delay $\tau_d = 0.1[s]$ (see Figs. 11a and 11c), $\tau_d = 0.6[s]$ (see Figs. 11b and 11d) and $\tau_d = 0.01[s]$ (see Fig. 11e). From Figs. 11a and 11b it is concluded that the robustness of the MPC strategy is higher than that of the other SCSs. As shown in Fig. 11b, there are almost no oscillations for the MPC based SCS, for a delay $\tau_d = 0.6[s]$, while the other control strategies have a noticeable oscillating behaviour.

Finally, comparing Fig. 11a and 11c, it is concluded that the dynamic performance is very similar for the cases of a step load connection (see Fig. 11a) and step load disconnection (see Fig. 11c).

VII. CONCLUSIONS

In this paper robust control methodologies for the secondary control of MGs have been presented. Two new SCS strategies based on Smith predictors and model predictive controllers have been analysed and tested using small signal analysis and simulation work. These control strategies have been designed to operate in MGs with variable and unknown communication delays with robust performance.

For the PI, SP and MPC strategies, the maximum delay achievable without obtaining unstable eigenvalues has been calculated in several operating points. From the stability analysis is concluded that the most robust performance is obtained using SCSs based on model predictive controllers.

A minor disadvantage of the MPC strategy is that the dynamic performance of this control method is slightly slower when compared to the PI and SP based SCSs when the design delay L is close to τ_d. However the MPC based SCS is considerably more robust in terms of maximum delay allowed.

Due to the robustness of the controller, it is concluded that MPC based secondary control system are the recommended control family to operate in systems where the communication delay is unknown with large variation values.

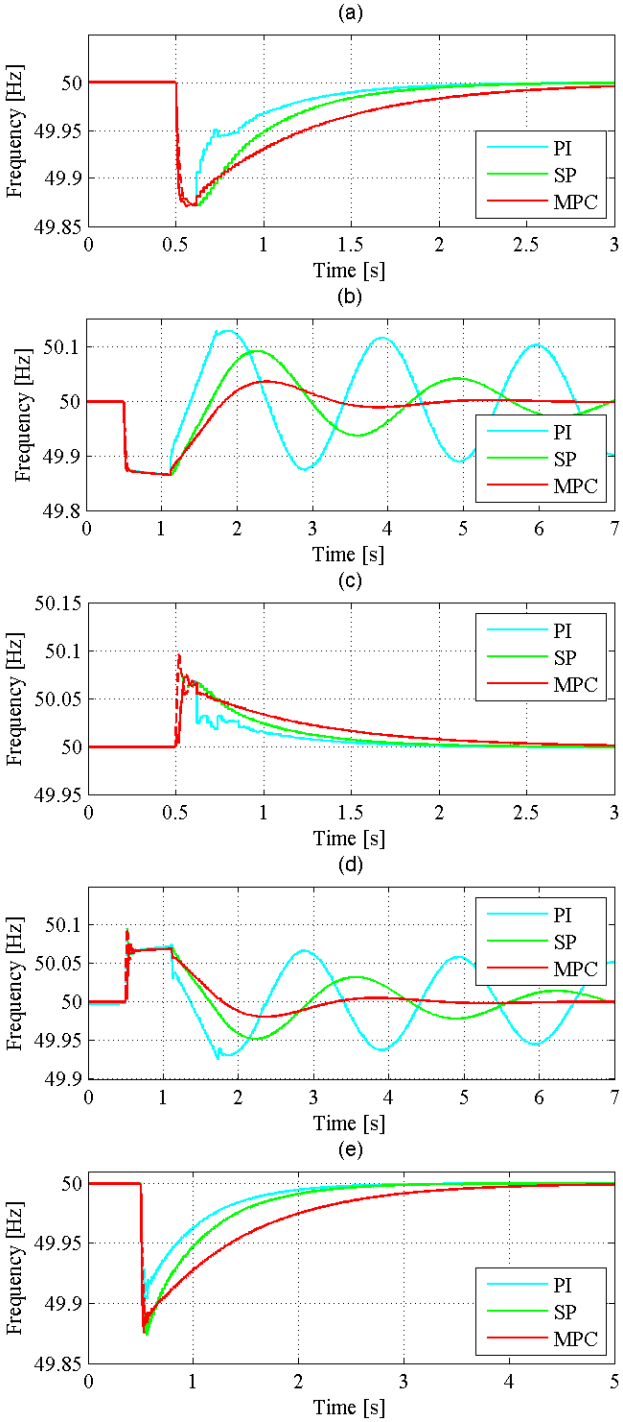

Fig. 11. Frequency from inverter 1 (continue line) and inverter 2 (dashed line) for a load connection with plant delay (a) $\tau_d = 0.1[s]$, and (b) $\tau_d = 0.6[s]$, for a load disconnection with plant delay (c) $\tau_d = 0.1[s]$, and (d) $\tau_d = 0.6[s]$, and (e) for a load connection with $\tau_d = 0.01[s]$ and $L = 0.2[s]$.

VIII. APPENDIX

A. SP Secondary control matrices

The matrices associated to the SP control as mentioned in section IV-B are the following:

$$A_{F_{SP}} = \begin{bmatrix} a_{11} & a_{12} & a_{13} & a_{14} & a_{15} \\ 1 & 0 & 0 & 0 & 0 \\ 0 & 1 & 0 & 0 & 0 \\ 0 & 0 & 1 & 0 & 0 \\ 0 & 0 & 0 & 1 & 0 \end{bmatrix}$$

$$B_{FP_{SP}} = [1 \quad 0 \quad 0 \quad 0 \quad 0]^T$$

With:

$$a_{11} = -\frac{L\tau\tau_d+2L\tau\tau_{PLL}+L\tau_d\tau_{PLL}+2\tau\tau_d\tau_{PLL}+K_pL\tau\tau_d}{L\tau\tau_d\tau_{PLL}}$$

$$a_{12}=-\frac{2L\tau+L\tau_d+2L\tau_{PLL}+2\tau\tau_d+4\tau\tau_{PLL}+2\tau_d\tau_{PLL}+2K_pL\tau+K_pL\tau_d+2K_p\tau\tau_d+K_iL\tau\tau_d}{L\tau\tau_d\tau_{PLL}}$$

$$a_{13} = -\frac{2L+4\tau+2\tau_d+4\tau_{PLL}+4K_p\tau-2K_p\tau_d+6K_pL+2K_iL\tau+K_iL\tau_d+2K_i\tau\tau_d}{L\tau\tau_d\tau_{PLL}}$$

$$a_{14} = -\frac{4K_p+4K_i\tau-2K_i\tau_d+6K_iL+4}{L\tau\tau_d\tau_{PLL}}$$

$$a_{15} = -\frac{4K_i}{L\tau\tau_d\tau_{PLL}}$$

B. Microgrid parameters

The following table present the load values for the two cases analysed.

TABLE V
LOADS VALUES

Case	Parameter	Value	Unit
Load Connection	Load 1 before impact	289.258+j18.1746	[VA]
	Load 2 before impact	289.258+j18.1746	[VA]
	Load impact 1	1799.93+j799.967	[VA]
	Load impact 2	1259.95+j1324.95	[VA]
Load Disconnection	Load 1 before impact	1799.93+j799.967	[VA]
	Load 2 before impact	1259.95+j1324.95	[VA]
	Load impact 1	1799.93+j799.967	[VA]
	Load impact 2	0	[VA]

C. Controllers values

The following tables present the values of the controllers used in the primary and secondary control respectively.

TABLE VI
PRIMARY CONTROLLERS VALUES

Controller	*Slope*	K_p	K_i
Inner Voltage	–	1.70	73
Inner Current	–	17.30	7208
Droop P-f	$6.98 * 10^{-4}$	–	–

TABLE VII
SECONDARY CONTROLLERS VALUES WITH SAMPLING TIME $T = 0.02[s]$

Controller	*Delay L [s]*	K_p	K_i	λ	N
PI	0.1	0.36	2.80	–	–
SP	0.1	0.12	3.16	–	–
MPC	0.1	–	–	224	15
PI	0.2	0.36	2.80	–	–
SP	0.2	0.12	3.16	–	–
MPC	0.2	–	–	97	15

IX. REFERENCES

[1]J. H. L. Kim, Jong-Yul; Park and Heung-Jae, "Coordinated Control Strategy for Microgrid in Grid-Connected and Islanded Operation," in *Proceedings of the 18th IFAC World Congress, 2011*, 2011, pp. 14766–14771.

[2]J. M. Guerrero, J. C. Vasquez, J. Matas, L. G. de Vicuna, and M. Castilla, "Hierarchical Control of Droop-Controlled AC and DC Microgrids; A General Approach Toward Standardization," *Ind. Electron. IEEE Trans.*, vol. 58, no. 1, pp. 158–172, 2011.

[3]T. L. Vandoorn, J. C. Vasquez, J. De Kooning, J. M. Guerrero, and L. Vandevelde, "Microgrids: Hierarchical Control and an Overview of the Control and Reserve Management Strategies," *Industrial Electronics Magazine, IEEE*, vol. 7, no. 4. pp. 42–55, 2013.

[4]A. Bidram and A. Davoudi, "Hierarchical Structure of Microgrids Control System," *Smart Grid, IEEE Transactions on*, vol. 3, no. 4. pp. 1963–1976, 2012.

[5]A. Madureira, C. Moreira, and J. P. Lopes, "Secondary Load-Frequency Control for MicroGrids in Islanded Operation," in *Proc. ICREPQ*, 2005.

[6]P. Borazjani, N. I. A. Wahab, H. B. Hizam, and A. Bt Che Soh, "A review on microgrid control techniques," *Innovative Smart Grid Technologies - Asia (ISGT Asia), 2014 IEEE*. pp. 749–753, 2014.

[7]D. E. Olivares, A. Mehrizi-Sani, A. H. Etemadi, C. A. Canizares, R. Iravani, M. Kazerani, A. H. Hajimiragha, O. Gomis-Bellmunt, M. Saeedifard, R. Palma-Behnke, G. A. Jimenez-Estevez, and N. D. Hatziargyriou, "Trends in Microgrid Control," *Smart Grid, IEEE Transactions on*, vol. 5, no. 4. pp. 1905–1919, 2014.

[8]J. M. Guerrero, J. Matas, L. G. de Vicuna, M. Castilla, and J. Miret, "Wireless-Control Strategy for Parallel Operation of Distributed-Generation Inverters," *Ind. Electron. IEEE Trans.*, vol. 53, no. 5, pp. 1461–1470, 2006.

[9]E. Planas, A. Gil-de-Muro, J. Andreu, I. Kortabarria, and I. M. de Alegria, "Stability analysis and design of droop control method in dq frame for connection in parallel of distributed energy resources," in *IECON 2012 - 38th Annual Conference on IEEE Industrial Electronics Society*, 2012, pp. 5683–5688.

[10] Y. Han, P. M. Young, A. Jain, and D. Zimmerle, "Robust Control for Microgrid Frequency Deviation Reduction With Attached Storage System," *Smart Grid, IEEE Transactions on*, vol. 6, no. 2. pp. 557–565, 2015.

[11] J. M. Guerrero, M. Chandorkar, T. Lee, and P. C. Loh, "Advanced Control Architectures for Intelligent Microgrids - Part I: Decentralized and Hierarchical Control," *Industrial Electronics, IEEE Transactions on*, vol. 60, no. 4. pp. 1254–1262, 2013.

[12] A. Micallef, M. Apap, C. Spiteri-Staines, J. M. Guerrero, and J. C. Vasquez, "Reactive Power Sharing and Voltage Harmonic Distortion Compensation of Droop Controlled Single Phase Islanded Microgrids," *Smart Grid, IEEE Transactions on*, vol. 5, no. 3. pp. 1149–1158, 2014.

[13] M. Savaghebi, A. Jalilian, J. C. Vasquez, and J. M. Guerrero, "Secondary Control for Voltage Quality Enhancement in Microgrids," *Smart Grid, IEEE Transactions on*, vol. 3, no. 4. pp. 1893–1902, 2012.

[14] T. L. Vandoorn, J. D. M. De Kooning, B. Meersman, J. M. Guerrero, and L. Vandevelde, "Voltage-Based Control of a Smart Transformer in a Microgrid," *Industrial Electronics, IEEE Transactions on*, vol. 60, no. 4. pp. 1291–1305, 2013.

[15] C. K. Sao, S. Member, and P. W. Lehn, "Voltage Source Converters," *IEEE Trans. Power Deliv.*, vol. 20, no. 2, pp. 1009–1016, 2005.

[16] A. Bidram, A. Davoudi, F. L. Lewis, and Z. Qu, "Secondary control of microgrids based on distributed cooperative control of multi-agent systems," *Generation, Transmission & Distribution, IET*, vol. 7, no. 8. pp. 822–831, 2013.

[17] A. Bidram, A. Davoudi, F. L. Lewis, and J. M. Guerrero, "Distributed Cooperative Secondary Control of Microgrids Using Feedback Linearization," *Power Systems, IEEE Transactions on*, vol. 28, no. 3. pp. 3462–3470, 2013.

[18] Q. Shafiee, J. M. Guerrero, and J. C. Vasquez, "Distributed Secondary Control for Islanded Microgrids--2014;A Novel Approach," *IEEE Trans. Power Electron.*, vol. 29, no. 2, pp. 1018–1031, 2014.

[19] J. A. P. Lopes, S. Member, C. L. Moreira, and A. G. Madureira, "Secondary Load-Frequency Control for MicroGrids in Islanded Operation," *IEEE trans. Power Syst.*, vol. 21, no. 2, pp. 916–924, 2006.

[20] X. Yu, X. She, X. Ni, and A. Q. Huang, "System Integration and Hierarchical Power Management Strategy for a Solid-State Transformer Interfaced Microgrid System," *Power Electronics, IEEE Transactions on*, vol. 29, no. 8. pp. 4414–4425, 2014.

[21] Q. Shafiee, J. M. Guerrero, and J. C. Vasquez, "Distributed Secondary Control for Islanded Microgrids - A Novel Approach," *Power Electronics, IEEE Transactions on*, vol. 29, no. 2. pp. 1018–1031, 2014.

[22] Y. Zhang and H. Ma, "Theoretical and Experimental Investigation of Networked Control for Parallel Operation of Inverters," *Industrial Electronics, IEEE Transactions on*, vol. 59, no. 4. pp. 1961–1970, 2012.
[23] C. Yuen, A. Oudalov, and A. Timbus, "The Provision of Frequency Control Reserves From Multiple Microgrids," *Industrial Electronics, IEEE Transactions on*, vol. 58, no. 1. pp. 173–183, 2011.
[24] S. K. Mazumder, M. Tahir, and K. Acharya, "Pseudo-decentralized control-communication optimization framework for microgrid: A case illustration," *Transmission and Distribution Conference and Exposition, 2008. IEEE/PES*. pp. 1–8, 2008.
[25] R. Palma-Behnke, C. Benavides, F. Lanas, B. Severino, L. Reyes, J. Llanos, D. Sáez, "A Microgrid Energy Management System Based on the Rolling Horizon Strategy", *Smart Grid, IEEE Trans.*, vol. 4, no. 2, pp. 996-1006, 2013.
[26] D. L. H. Aik and G. Andersson, "Use of participation factors in modal voltage stability analysis of multi-infeed HVDC systems," *Power Delivery, IEEE Transactions on*, vol. 13, no. 1. pp. 203–211, 1998.
[27] Q.-C. Zhong, "Robust Droop Controller for Accurate Proportional Load Sharing Among Inverters Operated in Parallel," *Industrial Electronics, IEEE Transactions on*, vol. 60, no. 4. pp. 1281–1290, 2013.
[28] J. Kim, J. M. Guerrero, P. Rodriguez, R. Teodorescu, and K. Nam, "Mode Adaptive Droop Control With Virtual Output Impedances for an Inverter-Based Flexible AC Microgrid," *Power Electron. IEEE Trans.*, vol. 26, no. 3, pp. 689–701, 2011.
[29] A. Engler and S. Energieversorgungstechnik, "Control of parallel operating battery inverters," *ISET Inst. für Solare Energieversorgungstechnik e.V.(EAWE)*, no. 49, pp. 1–4, 2000.
[30] A. Engler and N. Soultanis, "Droop control in LV-grids," in *Future Power Systems, 2005 International Conference on*, 2005, p. 6 pp.–6.
[31] X. Guo, Z. Lu, B. Wang, X. Sun, L. Wang, and J. M. Guerrero, "Dynamic Phasors-Based Modeling and Stability Analysis of Droop-Controlled Inverters for Microgrid Applications," *Smart Grid, IEEE Transactions on*, vol. 5, no. 6. pp. 2980–2987, 2014.
[32] T. C. Green and M. Prodanović, "Control of inverter-based micro-grids," *Electr. Power Syst. Res.*, vol. 77, no. 9, pp. 1204–1213, Jul. 2007.
[33] N. Pogaku, M. Prodanovic, and T. C. Green, "Modeling, Analysis and Testing of Autonomous Operation of an Inverter-Based Microgrid," *Power Electron. IEEE Trans.*, vol. 22, no. 2, pp. 613–625, 2007.
[34] F. Blaabjerg, R. Teodorescu, M. Liserre, and A. V Timbus, "Overview of Control and Grid Synchronization for Distributed Power Generation Systems," *Ind. Electron. IEEE Trans.*, vol. 53, no. 5, pp. 1398–1409, 2006.
[35] R. Cardenas, R. Pena, M. Perez, J. Clare, G. Asher, and F. Vargas, "Vector Control of Front-End Converters for Variable-Speed Wind-Diesel Systems," *IEEE Trans. Ind. Electron.*, vol. 53, no. 4, pp. 1127–1136, Jun. 2006.
[36] S. Ci, J. Qian, D. Wu, and A. Keyhani, "Impact of wireless communication delay on load sharing among distributed generation systems through smart microgrids," *Wireless Communications, IEEE*, vol. 19, no. 3. pp. 24–29, 2012.
[37] Q. Shafiee, C. Stefanovic, T. Dragicevic, P. Popovski, J. C. Vasquez, and J. M. Guerrero, "Robust Networked Control Scheme for Distributed Secondary Control of Islanded Microgrids," *Industrial Electronics, IEEE Transactions on*, vol. 61, no. 10. pp. 5363–5374, 2014.
[38] K. Watanabe and M. Ito, "A process-model control for linear systems with delay," *Automatic Control, IEEE Transactions on*, vol. 26, no. 6. pp. 1261–1269, 1981.
[39] A. Ingimundarson and T. Hägglund, "Robust tuning procedures of dead-time compensating controllers," *Control Eng. Pract.*, vol. 9, no. 11, pp. 1195–1208, Nov. 2001.
[40] R. Kennel, A. Linder, and M. Linke, "Generalized predictive control (GPC)-ready for use in drive applications?," *Power Electronics Specialists Conference, 2001. PESC. 2001 IEEE 32nd Annual*, vol. 4. pp. 1839–1844 vol. 4, 2001.
[41] D. W. Clarke, C. Mohtadi, and P. S. Tuffs, "Generalized predictive control—Part I. The basic algorithm," *Automatica*, vol. 23, no. 2, pp. 137–148, Mar. 1987.

Constanza Ahumada was born in Santiago, Chile. She received her B.Sc. degree and M.Sc. in electrical engineering from the University of Chile, 2011 and 2013, respectively. She is currently working toward the Ph.D. degree in the Faculty of Engineering from The University of Nottingham, Nottingham, U.K. Her main research interests are aerospace systems and renewable energy plants.

Roberto Cárdenas (S'95–M'97–SM'07) was born in Punta Arenas, Chile. He received the B.S. degree from the University of Magallanes, Punta Arenas, in 1988 and the M.Sc. and Ph.D. degrees from The University of Nottingham, Nottingham, U.K., in 1992 and 1996, respectively. From 1989 to 1991 and 1996 to 2008, he was a Lecturer with the University of Magallanes. From 1991 to 1996, he was with the Power Electronics Machines and Control Group (PEMC group), The University of Nottingham. From 2009 to 2011, he was with the Department of Electrical Engineering, University of Santiago, Santiago, Chile. He is currently a Professor in power electronics and drives with the Department of Electrical Engineering, University of Chile, Santiago. His main interests are in control of electrical machines, variable-speed drives, and renewable energy systems. Prof. Cárdenas was the recipient of the Best Paper Award from the IEEE TRANSACTIONS ON INDUSTRIAL ELECTRONICS in 2005.

Doris Sáez (S'93–M'96–SM'05) was born in Panguipulli, Chile. She received the M.Sc. and Ph.D. degrees in electrical engineering from the Pontificia Universidad Católica de Chile, in 1995 and 2000, respectively. She is currently an Associate Professor at the Department of Electrical Engineering, University of Chile. She is an Associate Editor of IEEE TRANSACTIONS ON FUZZY SYSTEMS. She is co-author of Springer-Verlag books: "Hybrid Predictive Control for Dynamic Transport Problems" (2013) and "Optimization of Industrial Processes at Supervisory Level: Application to Control of Thermal Power Plants" (2002). Her research fields are predictive control, fuzzy control design, fuzzy identification, control of renewable energy plants.

Josep M. Guerrero (S'01-M'04-SM'08-FM'15) received the B.S. degree in telecommunications engineering, the M.S. degree in electronics engineering, and the Ph.D. degree in power electronics from the Technical University of Catalonia, Barcelona, in 1997, 2000 and 2003, respectively. Since 2011, he has been a Full Professor with the Department of Energy Technology, Aalborg University, Denmark, where he is responsible for the Microgrid Research Program. From 2012 he is a guest Professor at the Chinese Academy of Science and the Nanjing University of Aeronautics and Astronautics; from 2014 he is chair Professor in Shandong University; and from 2015 he is a distinguished guest Professor in Hunan University.
His research interests is oriented to different microgrid aspects, including power electronics, distributed energy-storage systems, hierarchical and cooperative control, energy management systems, and optimization of microgrids and islanded minigrids. Prof. Guerrero is an Associate Editor for the IEEE TRANSACTIONS ON POWER ELECTRONICS, the IEEE TRANSACTIONS ON INDUSTRIAL ELECTRONICS, and the IEEE Industrial Electronics Magazine, and an Editor for the IEEE TRANSACTIONS on SMART GRID and IEEE TRANSACTIONS on ENERGY CONVERSION. He has been Guest Editor of the IEEE TRANSACTIONS ON POWER ELECTRONICS Special Issues: Power Electronics for Wind Energy Conversion and Power Electronics for Microgrids; the IEEE TRANSACTIONS ON INDUSTRIAL ELECTRONICS Special Sections: Uninterruptible Power Supplies systems, Renewable Energy Systems, Distributed Generation and Microgrids, and Industrial Applications and Implementation Issues of the Kalman Filter; and the IEEE TRANSACTIONS on SMART GRID Special Issue on Smart DC Distribution Systems. He was the chair of the Renewable Energy Systems Technical Committee of the IEEE Industrial Electronics Society. In 2014 he was awarded by Thomson Reuters as Highly Cited Researcher, and in 2015 he was elevated as IEEE Fellow for his contributions on "distributed power systems and microgrids."